Journal of Materials Chemistry A

RSC Publishing

PAPER

View Article Online
View Journal | View Issue

Cite this: J. Mater. Chem. A, 2013, 1, 9935

Probing the unusual anion mobility of $LiBH_4$ confined in highly ordered nanoporous carbon frameworks *via* solid state NMR and quasielastic neutron scattering

Xiangfeng Liu,*[ab] Eric H. Majzoub,*[a] Vitalie Stavila,[c] Raghunandan K. Bhakta,[c] Mark D. Allendorf,[c] David T. Shane,[d] Mark S. Conradi,[d] Nina Verdal,[e] Terrence J. Udovic[e] and Son-Jong Hwang[f]

Received 25th May 2013
Accepted 2nd July 2013

DOI: 10.1039/c3ta12051a

www.rsc.org/MaterialsA

Particle size and particle–framework interactions have profound effects on the kinetics, reaction pathways, and even thermodynamics of complex hydrides incorporated in frameworks possessing nanoscale features. Tuning these properties may hold the key to the utilization of complex hydrides in practical applications for hydrogen storage. Using carefully synthesized, highly-ordered, nanoporous carbons (NPCs), we have previously shown quantitative differences in the kinetics and reaction pathways of $LiBH_4$ when incorporated into the frameworks. In this paper, we probe the anion mobility of $LiBH_4$ confined in NPC frameworks by a combination of solid state NMR and quasielastic neutron scattering (QENS) and present some new insights into the nanoconfinement effect. NMR and QENS spectra of $LiBH_4$ confined in a 4 nm pore NPC suggest that the BH_4^- anions nearer the $LiBH_4$–carbon pore interface exhibit much more rapid translational and reorientational motions compared to those in the $LiBH_4$ interior. Moreover, an overly broadened BH_4^- torsional vibration band reveals a disorder-induced array of BH_4^- rotational potentials. XRD results are consistent with a lack of $LiBH_4$ long-range order in the pores. Consistent with differential scanning calorimetry measurements, neither NMR nor QENS detects a clear solid–solid phase transition as observed in the bulk, indicating that borohydride–framework interactions and/or nanosize effects have large roles in confined $LiBH_4$.

Introduction

Inducing changes in the thermodynamics and kinetics of materials at the nanoscale is increasingly important for energy storage materials such as pseudocapacitors, batteries, and hydrogen-storage materials. Increasing the charge and mass transport rates through shorter diffusion pathways allows for greater power in batteries and pseudocapacitors, and is also important in the complex metal hydrides, where the release or absorption of hydrogen requires mass transport and multi-step phase transformations.

Metal hydrides, sorbents, and chemical hydrides have been studied extensively in the last decade, yet hydrogen storage remains one of the key challenges to realizing the widespread commercialization of hydrogen-fueled technologies.[1–11] In spite of many achievements in hydrogen storage research, no material can meet all of the U.S. Department of Energy FreedomCAR requirements for vehicular transportation applications. Complex metal hydrides have received considerable attention owing to their high hydrogen capacity, but the high dehydrogenation temperatures and limited kinetics on hydriding have prevented their use in practical applications.[12–15] A few approaches have been applied to improve the kinetics and thermodynamics of complex metal hydrides as hydrogen storage materials.[16–21] The kinetics of hydrogen release and uptake in complex metal hydrides, such as $NaAlH_4$, are significantly improved by the addition of catalysts.[16,17] Furthermore, the addition of other reactants can act to "destabilize" the complex hydrides and improve the thermodynamics and reversibility. The best example of the latter is the addition of MgH_2 to $LiBH_4$, which forms MgB_2 on desorption,[18] but the dehydrogenation temperature remains too high for direct use of the waste heat from a proton exchange membrane (PEM) fuel cell. Recent studies show that nanoscale confinement of hydrides is potentially another important approach to improve both the kinetics and thermodynamics,[19–28] and theoretical calculations indicate that reducing the particle size of MgH_2 substantially decreases the H_2 desorption enthalpy.[29–32] More

[a]Center for Nanoscience, Department of Physics and Astronomy, University of Missouri-St. Louis, St. Louis, MO 63121, USA. E-mail: majzoube@umsl.edu
[b]College of Materials Science and Opto-Electronic Technology, University of Chinese Academy of Sciences, Beijing, 10049, P. R. China. E-mail: liuxf@ucas.ac.cn
[c]Sandia National Laboratories, Livermore, CA 94551-0969, USA
[d]Department of Physics, Washington University, St. Louis, MO 63130, USA
[e]NIST Center for Neutron Research, National Institute of Standards and Technology, Gaithersburg, MD 20899, USA
[f]Division of Chemistry and Chemical Engineering, California Institute of Technology, Pasadena, CA 91125, USA

recently, Fichtner *et al.* reported that the thermodynamic and kinetic properties of MgH_2 were both altered through nanoconfinement in activated carbon fiber (~3 nm).[33] The reaction enthalpy for the nanoconfined MgH_2 was reduced by 11 kJ mol^{-1} H_2, a significant effect. For some of the most desirable materials, such as $Mg(BH_4)_2$, (Mg and B are low-cost and readily available), tuning the kinetic and thermodynamic properties of complex hydrides through nanoscale confinement has become one of the most promising approaches to meet the targets necessary for widespread deployment of hydrides.[34]

In contrast to MgH_2, the complex metal hydrides undergo a dehydrogenation process that involves the breaking of covalent bonds in anionic complexes, such as BH_4^- and AlH_4^-.[35] The question naturally arises: does nanoconfinement of complex hydrides alter their thermodynamic stability? Fichtner *et al.* measured pressure-composition isotherms (PCI) of nanoconfined $NaAlH_4$ where no pressure plateau was observed, indicating a change in the local hydrogen environment with changing hydrogen concentration.[36] The lack of an observable plateau is similar in many respects to hydrogen pressure isotherms seen in metallic glasses and quasicrystals, where a broad distribution of hydrogen site energies precludes a flat plateau.[37] Interestingly, Bhakta *et al.* have shown that incorporation of $NaAlH_4$ in Cu–BTC (HKUST-1), a metal–organic framework with a pore size near 1.5 nm, shows an *increase* in the enthalpy of hydrogen desorption that is 7 kJ mol^{-1} H_2 greater than for the bulk, but with a reduced activation energy more than 60 kJ mol^{-1} H_2 lower than for the bulk.[38] The results indicate that not all complex metal hydrides behave similarly when confined in nanoframeworks. The effects of nanoconfinement on the phase transition, H_2 release/uptake, B_2H_6 emission, and reversibility of $LiBH_4$ have been systematically investigated in our earlier publications.[28,39] The results indicate that $LiBH_4$ confined in a highly-ordered, nanoporous carbon template has different kinetics and reaction pathway in comparison to the bulk sample. But the fundamental reasons for the differences are not very clear. Shane *et al.* studied the ion translational mobilities for $LiBH_4$ in carbon aerogels with average pore size diameters of 25 nm and 13 nm by solid state NMR and found enhanced anion and cation mobilities.[40] Two fractions of dynamically distinct BH_4^- were observed and attributed to more highly mobile BH_4^- anions in the surface or grain boundary regions of the nanoparticles and slower BH_4^- anions with more bulk-like mobilities in the nanoparticle interiors. Rapid Li^+ mobilities were found to persist even below the somewhat downshifted orthorhombic-to-hexagonal phase transition. Neutron scattering fixed-window scans (FWSs) of $LiBH_4$ in 13 nm carbon aerogels also measured enhanced BH_4^- reorientational mobilities compared to the bulk, especially for partially filled aerogels.[41] Verkuijlen *et al.* also studied structural and dynamical properties of $LiBH_4$ confined in a porous graphitic carbon and ordered porous silica by solid state NMR.[42] They found that the mobility of borohydride anions and lithium was strongly enhanced *via* the nanoconfinement of $LiBH_4$ in porous silica but a similar nanoconfinement effect in porous carbon was not directly observed because of line broading due to the carbon's magnetic susceptibility.[42] Nonetheless, using quasielastic neutron scattering (QENS), Remhof *et al.* recently reported the presence of reorientationally immobile BH_4^- anions as well as BH_4^- anions with relatively enhanced reorientational mobilities for $LiBH_4$ in this porous graphitic carbon.[43]

Understanding the effects of nanoconfinement on the ion mobility of complex metal hydrides might help to explain the nanoconfinement effects on the kinetics, reaction pathway and even the thermodynamic properties. In this study, we have probed the mobility of BH_4^- in $LiBH_4$ confined in a highly ordered nanoporous carbon (NPC) template through the combination of solid state NMR and quasielastic neutron scattering (QENS) and give some new insights into the effect of an ordered nanoporous carbon template on the structure and dynamic properties of $LiBH_4$.

Experimental

Carbon nanoframework synthesis

We prepared highly ordered and hexagonally packed cylindrical nanopores in hard carbon (NPC) frameworks according to a well-established method and incorporated $LiBH_4$ into the pores by melt infiltration.[39,44] The NPC-4 nm used in this study was prepared identically to that in our previous study, where 4 nm is the dominant pore size in the narrow distribution. The specific surface areas (S_{BET}) of NPC-4 nm based on the BET method and the total pore volume measured by the BJH method were 730 m^2 g^{-1} and 0.53 cm^3 g^{-1}, respectively.[39] The $LiBH_4$ loading was 20 mass%. This corresponds to a pore volume filling of 70%. One additional $LiBH_4$-infiltrated sample was dehydrided and rehydrided three times under 573 K and 60 bar H_2 and is referred to as the 'cycled' sample.

Magnetic resonance

Static-sample ^1H NMR was performed in a 2.0 Tesla, NMR-stabilized electromagnet at 85.03 MHz. Spectra were obtained with short (1 or 2 microsecond) rf pulses to minimize spectral distortions. The portion of the free induction decay obscured by ringing after the rf pulse (first 2 microseconds) was supplied by Gaussian back-extrapolation from the observed signal. Temperatures were regulated by a stream of thermostated air and measured with a thermocouple near the sample. Multinuclear solid state magic-angle spinning (MAS) nuclear magnetic resonance (NMR) spectra were obtained using a Bruker DSX-500 spectrometer and a Bruker 4 mm probe. The operating frequencies for ^1H, ^{11}B, and ^7Li are 500.2, 160.5, and 194.4 MHz, respectively. A sample in powder form was packed into a 4 mm ZrO_2 rotor and sealed with a tightly fitting kel-F cap inside an argon glove box, and was spun at 15 kHz using compressed dry N_2 gas in order to avoid any contact with oxygen or moisture. Quartz glass powder was often mixed as a diluting agent when the electrically conducting nature of the sample caused severe probe detuning problems. NMR spectra were referenced to external references of tetramethylsilane (TMS), $BF_3 \cdot O(CH_2CH_3)_2$, and 1 M aqueous solution of LiCl for ^1H, ^{11}B, and ^7Li, respectively.

Neutron spectroscopy

All neutron scattering measurements were performed at the National Institute of Standards and Technology (NIST) Center for Neutron Research. Fixed-window-scan measurements were performed on the High Flux Backscattering Spectrometer[45] (HFBS) with an incident neutron wavelength of 6.27 Å (2.08 meV) and a resolution of 0.8 μeV full width at half maximum (FWHM). Quasielastic neutron scattering (QENS) spectra were collected on the Disc Chopper Spectrometer[46] (DCS) with incident neutron wavelengths of 2.75 Å (10.8 meV, with 275 μeV FWHM elastic linewidth), 5 Å (3.3 meV, with 50.1 μeV FWHM and 105.5 μeV FWHM elastic linewidths), and 8 Å (1.3 meV with 14.3 μeV FWHM elastic linewidth). The QENS spectra were reduced and analyzed using the DAVE[47] software package. Neutron vibrational spectroscopy (NVS) measurements were collected at 4 K in neutron energy loss on the Filter Analyzer Neutron Spectrometer[48] (FANS) with pre- and post-monochromator collimations of 60′ and 40′, respectively, resulting in an instrumental resolution between 1.5 meV and 16 meV over the vibrational energy range (34 meV to 200 meV) presented. Isotopically labeled $^{7}Li^{11}BH_4$ was used as the infiltrant in the neutron scattering experiments to avoid the strong neutron absorption of ^{10}B and ^{6}Li isotopes.

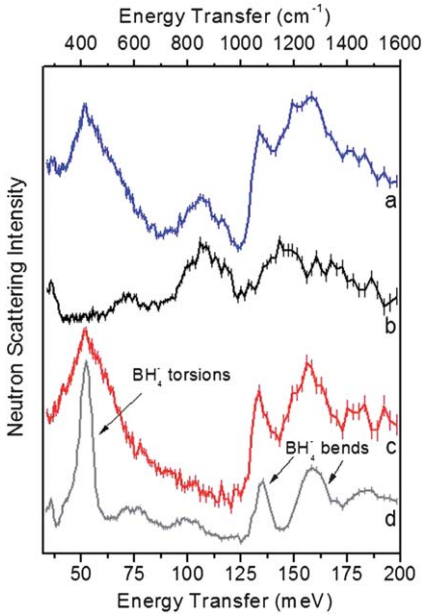

Fig. 1 Neutron vibrational spectra for (a) $LiBH_4$@NPC-4 nm (blue), (b) the empty framework, NPC-4 nm (black), (c) $LiBH_4$@NPC-4 nm minus NPC-4 nm (red), and (d) bulk $LiBH_4$ (gray). An overly broadened BH_4^- torsional band for $LiBH_4$@NPC-4 nm centered at 52 meV (419 cm^{-1}) clearly indicates a non-bulk-like distribution of BH_4^- rotational potentials due to structural disorder.

Results

We previously characterized the $LiBH_4$-infiltrated NPC through FTIR spectroscopy, X-ray diffraction (XRD), and differential scanning calorimetry (DSC).[28,39] FTIR spectra indicate that a large fraction of the BH_4^- anions remain intact, as evidenced by the presence of B–H stretching and bending modes. XRD indicates that the $LiBH_4$ lacks long-range order, as indicated by the absence of Bragg peaks. Additionally, DSC indicates the absence of both the orthorhombic to hexagonal structural transition and melting peaks at about 388 K and 557 K, respectively.

Neutron vibrational spectra for bulk $LiBH_4$ and $LiBH_4$@NPC-4 nm at 4 K are shown in Fig. 1. The spectrum (curve b) for the empty 4 nm NPC reveals the vibrational density of states for residual hydrogen. The spectrum strongly resembles that of other hydrogenous disordered carbons and the polycyclic aromatic hydrocarbon coronene[48] and likely reflects sp^2-hybridized C–H edge groups decorating graphene-like fragments. Neutron prompt gamma activation analysis[49] indicates an H/C atom ratio of ~0.1. A comparison of the vibrational spectra for nano-sequestered (minus the NPC spectrum) (curve c) and bulk $LiBH_4$ (curve d) corroborates that the hydrogen atoms present in the NPC pores (unlike the H atoms associated with the empty NPC) are predominantly associated with $LiBH_4$.[50] The bending mode vibrations (between 125 meV and 180 meV) of the BH_4^- anions do not change much upon infiltration. Nonetheless, an overly broadened BH_4^- torsional band for $LiBH_4$@NPC-4 nm centered at 52 meV (419 cm^{-1}) clearly indicates a non-bulk-like distribution of BH_4^- rotational potentials due to structural disorder.

A distinguishing feature of the infiltrated hydride materials is the resulting dynamics of BH_4^- "interface" anions that are in close proximity to the pore walls. It is evident that, as the pores become narrower, the prevalence of more rapid, non-bulk-like BH_4^- motions increases, as indicated by static-sample (not magic-angle spinning) hydrogen NMR. In particular, Fig. 2a shows room-temperature ^1H NMR spectra of three different materials: bulk $LiBH_4$, $LiBH_4$ in a carbon aerogel with 13 nm diameter pores,[40] and $LiBH_4$ in NPC-4 nm. Generally, a narrower line corresponds to faster H motion (motional averaging of the nuclear spin dipolar interactions). The bulk spectrum shows a single broad line (no mobile BH_4^- anions), whereas the aerogel spectrum shows a broad component and a narrow component. The narrow component corresponds to more mobile BH_4^- anions near the carbon–$LiBH_4$ interface, while the broad component corresponds to BH_4^- anions in the interior of the $LiBH_4$, which behave more bulk-like. We note that a melting peak in DSC for crystalline $LiBH_4$ is still visible in the infiltrated 13 nm aerogel sample.[23] The NPC-4 nm sample also has narrow and broad NMR components, but the narrow component is now even more dominant, indicating that an even greater fraction of the BH_4^- anions are mobile. Note that we are referring to translational mobility on the timescale of NMR lineshapes (10^{-5} s); even in bulk $LiBH_4$, all the BH_4^- anions reorient in place rapidly already at 138 K.[40] Fig. 2b shows the NPC-4 nm spectra at different temperatures and indicates that the translational motional narrowing is frozen out at low temperature (137 K). One may argue that being within 2 nm or less of a pore wall (the radius of the pores in the NPC-4 nm) produces either some change in $LiBH_4$ coordination or an interaction with the framework wall that results in faster H motion. The translationally distinct populations of BH_4^- anions also likely possess corresponding variations in their reorientational jump rates as

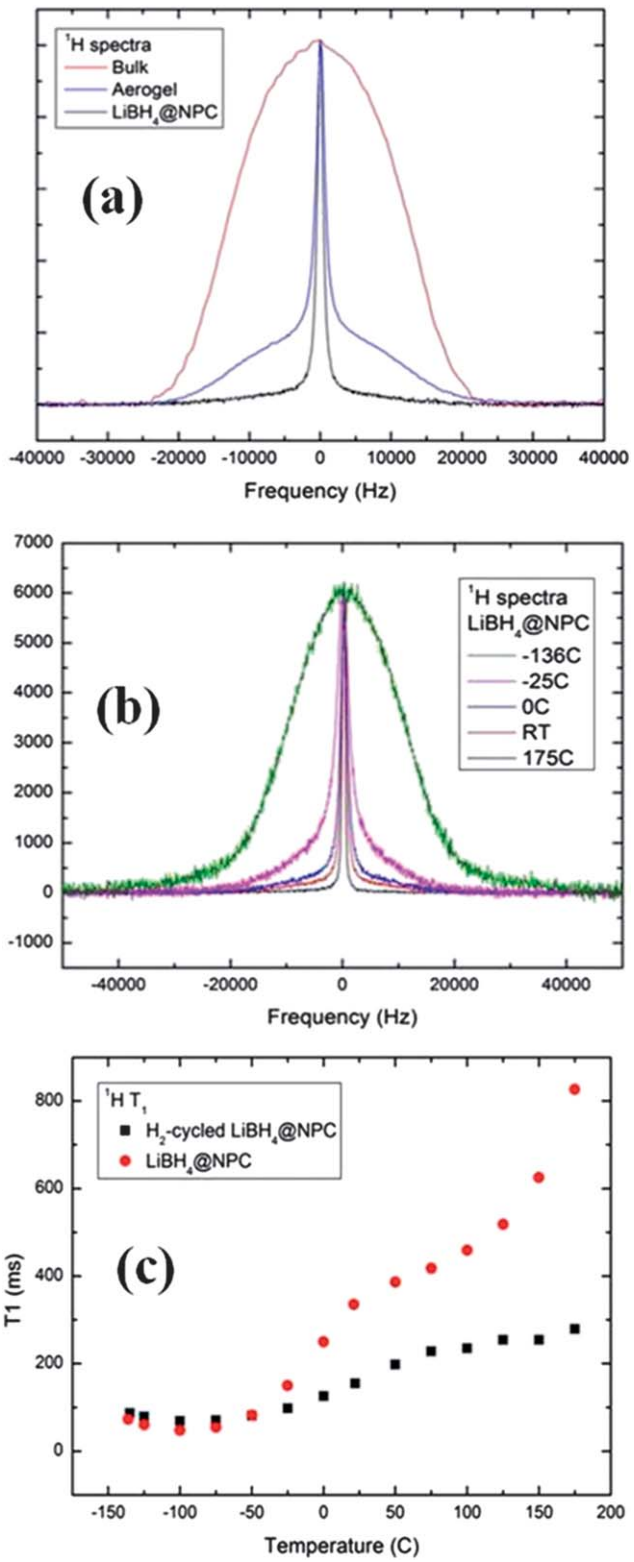

Fig. 2 (a) Room-temperature ^{1}H NMR lineshapes for $LiBH_4$ bulk (red), $LiBH_4$ infiltrated in 13 nm aerogel (blue),[40] and $LiBH_4$ infiltrated in NPC-4 nm (black). (b) ^{1}H NMR lineshapes for $LiBH_4$ infiltrated in NPC-4 nm at several different temperatures, indicating motional narrowing at higher temperatures. The temperatures of the curves are −136 °C, −25 °C, 0 °C, 23 °C, and 175 °C from-broadest to narrowest NMR. (c) Spin-lattice (T_1) relaxation time for $LiBH_4$@NPC-4 nm (red circles). Hydrogen cycled sample data are black squares.

suggested by the QENS measurements discussed below. Fig. 2c shows the spin-lattice (T_1) ^{1}H relaxation time as a function of temperature. Generally one obtains a minimum in the T_1 when fluctuations in the dipolar interactions between the spins occur at a rate equal to the Larmor frequency of the spin (in this case, 10^9 s^{-1}). For example, for the ^{1}H T_1 in bulk $LiBH_4$, one observes a minimum around 173 K (−100 °C) caused by BH_4 reorientations.[40] This minimum is also visible (Fig. 2c) in $LiBH_4$@NPC-4 nm, demonstrating that many of the BH_4^- anions reorient at rates similar to the anions in bulk $LiBH_4$. Bulk $LiBH_4$ also shows a discontinuity in T_1 around 383 K at the solid–solid phase transition. This transition is absent in $LiBH_4$@NPC-4 nm. Finally, in bulk $LiBH_4$ there is a second, shallower minimum around 448 K caused by the rapid lithium motion that begins at the solid–solid phase transition. Fig. 2c still indicates a "dip" in the ^{1}H T_1 data for $LiBH_4$@NPC-4 nm with increasing temperature near 373 K, but it is not as pronounced as in the bulk and it starts at a lower temperature, probably because the lithium motion is already fast at a lower temperature. The cycled-sample data are flatter, suggesting a wider distribution of motion rates and, in part, chemical transformation of some of the $LiBH_4$.

Neutron scattering fixed-window scans for bulk $LiBH_4$ and $LiBH_4$@NPC-4 nm, collected on HFBS, are shown in Fig. 3. At the lowest temperatures, the maximum elastic intensity reflects the fact that all BH_4^- anions are "rotationally immobile" on the HFBS timescale ($<10^{-8}$ reorientations per s). As the temperature is increased, the dramatic drop in elastic intensity indicates the onset of BH_4^- "rotational mobility" (*i.e.*, a change of some resolution-limited elastic intensity to more broadened quasie-lastic intensity, reflecting BH_4^- reorientational motions). It is clear that the onset occurs near 50 K for the confined $LiBH_4$, about 100 K lower than for the bulk (near 150 K), in agreement with observations in NMR and consistent with the FWS behavior of BH_4^- anions observed for $LiBH_4$ in 13 nm carbon aerogels.[41] Furthermore, the onset of BH_4^- rotational dynamics in the NPC is more gradual than in the bulk, suggesting an inhomogeneity (broad distribution) in the BH_4^- rotational potentials for the former.

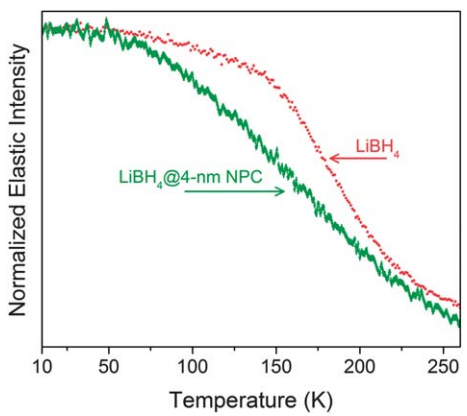

Fig. 3 A comparison of the elastic scattering intensity *vs.* temperature for $LiBH_4$@NPC-4 nm and bulk $LiBH_4$ on HFBS.

Consistent with NMR observations of two translationally distinct BH_4^- populations in $LiBH_4$@NPC-4 nm, analysis of QENS spectra reveal two reorientationally distinct populations of BH_4^- anions. Such a spectrum at 400 K is shown in Fig. 4. The quasielastic scattering from this material is best represented by two Lorentzian functions, with linewidths differing by nearly an order of magnitude. Analogous to the translationally slower interior and more rapid interface BH_4^- anions observed by NMR, the narrower and broader Lorentzian components are associated with the reorientational motions of the less mobile, more bulk-like interior and more mobile, interface BH_4^- anions, respectively. Activation energies for reorientation of 16 ± 1 kJ mol^{-1} and 10.6 ± 0.7 kJ mol^{-1} for the relatively less and relatively more mobile BH_4^- populations were determined from an Arrhenius plot of the Lorentzian linewidths. For the former and latter populations, respectively, the reorientation jump rates from the Arrhenius fits varied from $\sim 2.6 \times 10^9$ s^{-1} and 5.6×10^{10} s^{-1} at 193 K to $\sim 3.5 \times 10^{11}$ s^{-1} and 2.1×10^{12} s^{-1} at 400 K. The reorientation rates and activation energy of the less mobile population are in reasonable agreement with what is observed with QENS for bulk $LiBH_4$ ($E_a = 17.3 \pm 0.3$ kJ mol^{-1} from Remhof *et al.*[51]). The rather well-behaved Arrhenius dependences of the two Lorentzian components from 193 K to 400 K appear to be inconsistent with the presence of a solid–solid phase transition in this region. The two dynamically distinct components observed in the present NMR and QENS study are somewhat at odds with the one Lorentzian component observed in the recent QENS study of $LiBH_4$ confined in a porous graphitic carbon with a 10 nm diameter average pore size.[43] Since the quasielastic linewidth in the latter study lies somewhere between the linewidths of the two QENS components for the $LiBH_4$@NPC-4 nm, we suggest that this single Lorentzian feature may merely be reflecting an average linewidth due to reorientationally slower interior and reorientationally faster interface anions. A more detailed analysis of nanoconfined $LiBH_4$ reorientational behavior based on our QENS results is beyond the scope of this paper and will be published separately.

Similarly, multinuclear high-resolution NMR spectra of the $LiBH_4$@NPC-4 nm sample show two different kinds of peaks,

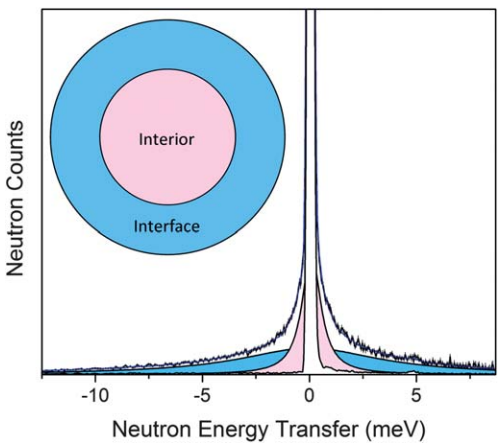

Fig. 4 Quasielastic neutron scattering spectrum of $LiBH_4$@NPC-4 nm at 400 K and 3 Å^{-1} momentum transfer. The spectrum is fit to an elastic line with instrumental resolution (white) and two Lorentzian functions (narrower: pink and broader: blue) that reflect two different BH_4^- reorientational dynamics. The inserted schematic indicates a cross section of a 4 nm pore with two layers of $LiBH_4$ (interface: blue and interior: pink). The faster component is in blue and the slower is in pink.

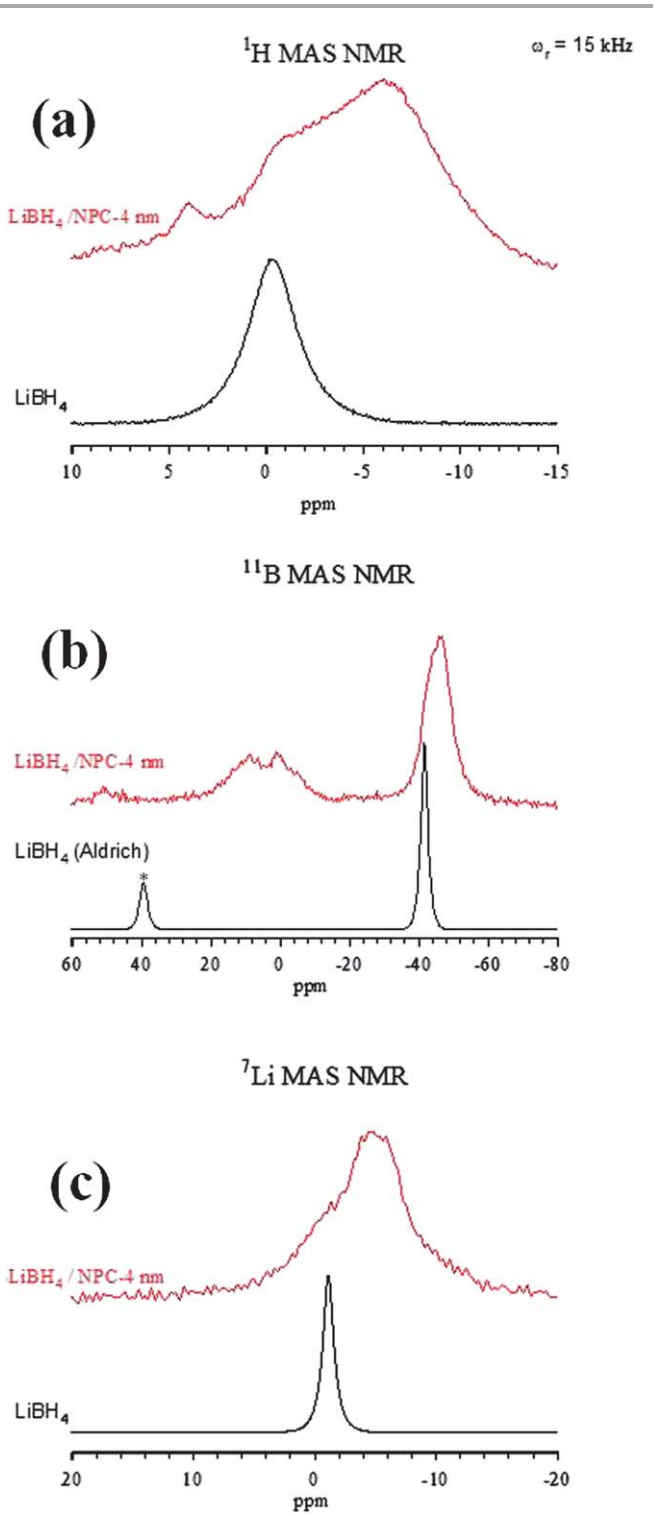

Fig. 5 MAS NMR spectra of $LiBH_4$@NPC-4 nm (a) ^{1}H, (b) ^{11}B, and (c) ^{7}Li in comparison with those of bulk $LiBH_4$ (Sigma-Aldrich). The sample spinning rate was 15 kHz and spinning sidebands are marked with an *.

with one shifted upfield (by 4–5 ppm to lower value in ppm) while the other is broadened but remains at the same position as in bulk $LiBH_4$ (see Fig. 5). This behavior is consistent in magnitude and spectral shape for all three nuclei measured and suggests $LiBH_4$ in two distinct environments: (i) material near the pore wall and less bulk-like, or (ii) further from the pore wall (the pore interior) and more bulk-like. The similar effect on all 3 nuclei demonstrates that $LiBH_4$ near the pore wall appears to experience a shift of the B-field from anisotropic magnetic susceptibility of the sp^2-carbon matrix that is not fully averaged by MAS.[52] Peak decomposition of ^{11}B allowed us to estimate that about 50% of ^{11}B spins are BH_4 near the pore wall, and 10% are BH_4 near the center of the pore and more bulk-like. ^{11}B NMR spectra also showed sizeable peaks in the 20 ppm to −10 ppm range, indicating that about 40% of ^{11}B atoms experienced chemical transformation such as oxidation during the infiltration process. Note that a sharp peak at 4 ppm in the ^1H MAS spectrum is due to H_2 gas.

In a simple hydride such as MgH_2, nanoparticles contain many surface H atoms with low coordination, and necessarily higher energy than subsurface H, where the coordination number is higher and the arrangement is more bulk-like.[29] For complex hydrides such as $LiBH_4$ or $NaAlH_4$, hydrogen is covalently bound in a tetrahedral coordination to a central atom (*e.g.* $[AlH_4]^-$, $[BH_4]^-$), even at the interfaces with the framework. In contrast to MgH_2, the dehydrogenation process of complex hydrides must involve the bond-breaking of intact anionic complexes, even if the (surface or near-surface) anion complex has an altered coordination number. If nanoconfinement does not fundamentally change the local hydrogen environment by altering bond energies of the complex, it follows that the enthalpy may not be significantly altered, provided the product phase(s) in the desorbed material are identical.

Conclusions

In summary, the structure and dynamic properties of $LiBH_4$ confined in highly ordered nanoporous carbon templates with cylindrical pores with an average pore size of 4 nm have been investigated by means of solid state NMR, NVS, and QENS. Nuclear magnetic resonance and neutron scattering data suggest that BH_4^- anion translational and reorientational mobility is significantly enhanced in $LiBH_4$ as the particle size is reduced by confinement in the NPC-4 nm carbon. The more highly (translationally and reorientationally) mobile BH_4^- anions are believed to be located in the $LiBH_4$ interface region with the pore wall. In contrast, the slower anions with more bulk-like mobilities are believed to be located in the pore interiors. Neither NMR nor QENS detects a clear solid–solid phase transition of $LiBH_4$ confined in NPC as observed in the bulk, indicating that hydride–framework interactions and/or nanoscale size effects play a large role in confined $LiBH_4$.

Acknowledgements

This work was funded by the U.S. Department of Energy in the Hydrogen, Fuel Cells, and Infrastructure Technologies Program through the office Energy Efficiency and Renewable Energy. This work utilized facilities supported in part by the National Science Foundation under Agreement DMR-0944772. This work was partially supported by DOE-EERE under Agreement no. DE-EE0002978. The work at Washington University was supported by DOE Basic Energy Sciences grant DE-FG02-05ER46256. The NMR facility at Caltech was supported by the National Science Foundation (NSF) under Grant Number 9724240 and partially supported by the MRSEC Program of the NSF under Award Number DMR-520565. The work at University of Chinese Academy of Sciences was supported by "Hundred Talents Project" and the National Basic Research Program of China (973 Program, 2010CB833101).

References

1 L. Schlapbach and A. Züttel, *Nature*, 2001, **414**, 353–358.
2 P. Chen and M. Zhu, *Mater. Today*, 2008, **11**, 36–43.
3 U. Eberle, M. Felderhoff and F. Schuth, *Angew. Chem., Int. Ed.*, 2009, **48**, 6608–6630.
4 J. Graetz, *Chem. Soc. Rev.*, 2009, **38**, 73–82.
5 H. W. Li, Y. Yan, S. Orimo, A. Züttel and C. M. Jensen, *Energies*, 2011, **4**, 185–214.
6 H. Reardon, J. M. Hanlon, R. W. Hughes, A. Godula-Jopek, T. K. Mandal and D. H. Gregory, *Energy Environ. Sci.*, 2012, **5**, 5951–5979.
7 H. Shao, G. Xin, J. Zheng, X. Li and E. Akiba, *Nano Energy*, 2012, **1**, 590–601.
8 Y. Li, F. Fang, H. Fu, J. Qiu, Y. Song, Y. Li, D. Sun, Q. Zhang, L. Ouyang and M. Zhu, *J. Mater. Chem. A*, 2013, **1**, 5238–5246.
9 P. Wang and C. M. Jensen, *J. Phys. Chem. B*, 2004, **108**, 15827–15829.
10 J. Gu, M. Gao, H. Pan, Y. Liu, B. Li, Y. Yang, C. Liang, H. Fu and Z. Guo, *Energy Environ. Sci.*, 2013, **6**, 847–858.
11 T. D. Humphries, D. Birkmire, B. C. Hauback, G. S. McGrady and C. M. Jensen, *J. Mater. Chem. A*, 2013, **1**, 2974–2977.
12 S. Orimo, Y. Nakamori, J. R. Eliseo, A. Züttel and C. M. Jensen, *Chem. Rev.*, 2007, **107**, 4111–4132.
13 F. Schüth, B. Bogdanović and M. Felderhoff, *Chem. Commun.*, 2004, 2249–2258.
14 W. Grochala and P. P. Edwards, *Chem. Rev.*, 2004, **104**, 1283–1315.
15 J. Lu, Z. Z. Fang, Y. J. Choi and H. Y. Sohn, *J. Phys. Chem. C*, 2007, **111**, 12129–12134.
16 B. Bogdanović and M. Schwickardi, *J. Alloys Compd.*, 1997, **253**, 1–9.
17 J. Shao, X. Xiao, L. Chen, X. Fan, S. Li, H. Ge and Q. Wang, *J. Mater. Chem.*, 2012, **22**, 20764–20772.
18 J. J. Vajo, S. L. Skeith and F. Mertens, *J. Phys. Chem. B*, 2005, **109**, 3719–3722.
19 S. Zheng, F. Fang, G. Zhou, G. Chen, M. Zhu and D. Sun, *Chem. Mater.*, 2008, **20**, 3954–3958.
20 C. P. Balde, B. P. C. Hereijgers, J. H. Bitter and K. P. de Jong, *J. Am. Chem. Soc.*, 2008, **130**, 6761–6765.
21 X. Liu, D. Peaslee and E. H. Majzoub, *J. Mater. Chem. A*, 2013, **1**, 3926–3931.
22 J. J. Vajo, *Curr. Opin. Solid State Mater. Sci.*, 2011, **15**, 52–61.

23 A. F. Gross, J. J. Vajo, S. L. Van Atta, G. L. Olson, S. L. Skeith and F. Mertens, *J. Phys. Chem. C*, 2008, **112**, 5651–5657.
24 P. Adelhelm, J. Gao, M. H. W. Verkuijlen, C. Rongeat, M. Herrich, P. J. M. van Bentum, O. Gutfleisch, A. P. M. Kentgens, K. P. de Jong and P. E. de Jongh, *Chem. Mater.*, 2010, **22**, 2233–2238.
25 J. Gao, P. Adelhelm, M. H. W. Verkuijlen, C. Rongeat, M. Herrich, P. J. M. van Bentum, O. Gutfleisch, A. P. M. Kentgens, K. P. de Jong and P. E. de Jongh, *J. Phys. Chem. C*, 2010, **114**, 4675–4682.
26 G. Xia, L. Li, Z. Guo, Q. Gu, Y. Guo, X. Yu, H. Liu and Z. Liu, *J. Mater. Chem. A*, 2013, **1**, 250–257.
27 T. K. Nielsen, U. Bösenberg, R. Gosalawit, M. Dornheim, Y. Cerenius, F. Besenbacher and T. R. Jensen, *ACS Nano*, 2010, **4**, 3903–3908.
28 X. Liu, D. Peaslee, C. Z. Jost and E. H. Majzoub, *J. Phys. Chem. C*, 2010, **114**, 14036–14041.
29 R. W. P. Wagemans, J. H. van Lenthe, P. E. de Jongh, A. Jos van Dillen and K. P. de Jong, *J. Am. Chem. Soc.*, 2005, **127**, 16675–16680.
30 M. Paskevicius, D. A. Sheppard and C. E. Buckley, *J. Am. Chem. Soc.*, 2010, **132**, 5077–5083.
31 Z. G. Wu, M. D. Allendorf and J. C. Grossman, *J. Am. Chem. Soc.*, 2009, **131**, 13918–13919.
32 L. K. Wagner, E. H. Majzoub, M. D. Allendorf and J. C. Grossman, *Phys. Chem. Chem. Phys.*, 2012, **14**, 6611–6616.
33 Z. Zhao-Karger, J. Hu, A. Roth, D. Wang, C. Kubel, W. Lohstroh and M. Fichtner, *Chem. Commun.*, 2010, **46**, 8353–8355.
34 T. K. Nielsen, F. Besenbacher and T. R. Jensen, *Nanoscale*, 2011, **3**, 2086–2098.
35 J. Yang, A. Sudik, C. Wolverton and D. J. Siegel, *Chem. Soc. Rev.*, 2010, **39**, 656–675.
36 W. Lohstroh, A. Roth, H. Hahn and M. Fichtner, *ChemPhysChem*, 2010, **11**, 789–792.
37 V. T. Huett, D. Zander, L. Jastrow, E. H. Majzoub, K. F. Kelton and U. Köster, *J. Alloys Compd.*, 2004, **379**, 16–22.
38 R. K. Bhakta, S. Maharrey, V. Stavila, A. Highley, T. Alam, E. H. Majzoub and M. Allendorf, *Phys. Chem. Chem. Phys.*, 2012, **14**, 8160–8169.
39 X. Liu, D. Peaslee, C. Z. Jost, T. F. Baumann and E. H. Majzoub, *Chem. Mater.*, 2011, **23**, 1331–1336.
40 D. T. Shane, R. L. Corey, C. McIntosh, L. H. Rayhel, Jr, R. C. Bowman, J. J. Vajo, A. F. Gross and M. S. Conradi, *J. Phys. Chem. C*, 2010, **114**, 4008–4014.
41 T. J. Udovic, N. Verdal, J. J. Rush, D. J. D. Vries, M. R. Hartman, J. J. Vajo, A. F. Gross and A. V. Skripov, *J. Alloys Compd.*, 2013, DOI: 10.1016/j.jallcom.2013.02.025, in press.
42 M. H. W. Verkuijlen, P. Ngene, D. W. de Kort, C. Barre, A. Nale, E. R. H. van Eck, P. J. M. van Bentum, P. E. de Jongh and A. P. M. Kentgens, *J. Phys. Chem. C*, 2012, **116**, 22169–22178.
43 A. Remhof, P. Mauron, A. Züttel, J. P. Embs, Z. Łodziana, A. J. Ramirez-Cuesta, P. Ngene and P. de Jongh, *J. Phys. Chem. C*, 2013, **117**, 3789–3798.
44 Y. Meng, D. Gu, F. Zhang, Y. Shi, L. Cheng, D. Feng, Z. Wu, Z. Chen, Y. Wan, A. Stein and D. Zhao, *Chem. Mater.*, 2006, **18**, 4447–4464.
45 A. Meyer, R. M. Dimeo, P. M. Gehring and D. A. Neumann, *Rev. Sci. Instrum.*, 2003, **74**, 2759–2777.
46 J. R. D. Copley and J. C. Cook, *Chem. Phys.*, 2003, **292**, 477–485.
47 R. Azuah, L. Kneller, Y. Qiu, P. L. W. Tregenna-Piggott, C. Brown, J. Copley and R. Dimeo, *J. Res. Natl. Inst. Stand. Technol.*, 2009, **114**, 341–358.
48 T. J. Udovic, C. M. Brown, J. B. Leão, P. C. Brand, R. D. Jiggetts, R. Zeitoun, T. A. Pierce, I. Peral, J. R. D. Copley, Q. Huang, D. A. Neumann and R. J. Fields, *Nucl. Instrum. Methods Phys. Res., Sect. A*, 2008, **588**, 406–413.
49 R. L. Paul and R. M. Lindstrom, *J. Radioanal. Nucl. Chem.*, 2000, **243**, 181–189.
50 M. R. Hartman, J. J. Rush, T. J. Udovic, R. C. Bowman Jr and S.-J. Hwang, *J. Solid State Chem.*, 2007, **180**, 1298–1305.
51 A. Remhof, Z. Łodziana, P. Martelli, O. Friedrichs, A. Züttel, A. V. Skripov, J. P. Ebbs and T. Strässle, *Phys. Rev. B: Condens. Matter Mater. Phys.*, 2010, **81**, 214304.
52 D. L. Van der Hart, W. L. Earl and A. N. Garroway, *J. Magn. Reson.*, 1981, **44**, 361–401.